Electron multiplying CCDs for sensitive wavefront sensing at 3k frames per second

Émile Beaulieu[a], Yoann Gosselin[a], Jérémy Tucotte[a], Arnaud Symon[a], Abtin Ghodoussi[a], and Olivier Daigle[a]

[a]Nüvü Caméras Inc., 603-355 rue Peel, Montréal, QC, Canada, H3C 2G9

ABSTRACT

The science goals of current and upcoming large telescopes require the highest level of adaptive optics (AO) performance. To address these requirements, an electron-multiplying CCD (EMCCD), the HNü240, has been developed based on the Teledyne-e2v CCD220 240x240 pixel detector with Nüvü Caméras' re-designed EMCCD electronics. The HNü240 delivers a full-detector frame rate of up to 3015 frames per second with 35.5 μs first-pixel latency, sub-electron noise and flexible readout sequences that can be tailored to different wavefront sensor designs. The sealed-body design and fully airless cooling prevent unwanted airflow while eliminating thermal gradients on the camera body. Details of the HNü240's design, performance results and applications to AO systems in exoplanet detection, quantum key distribution and space situational awareness will be discussed.

Keywords: EMCCD, Adaptive Optics, Wavefront Sensing, Photon Counting

1. INTRODUCTION

As telescope technologies evolve, more & more research areas depend on higher-quality images. Adaptive Optics (AO) are currently a major factor in improving ground-based acquisitions, even recently seeing implementation in space-based imaging missions [1]. This in turn is driving demand for sensitive Wavefront Sensor (WFS) that not only detect higher order aberrations with a limited number of photons but also run at higher frame rates to outpace the changing atmosphere.

Achieving these goals requires larger, faster and more sensitive cameras. Teledyne-e2v's CCD220 is an attractive detector to fulfill these needs, with a 240 $\times$ 240 pixel imaging area and high-speed multi-output split-frame transfer design combined with the Electron Multiplying CCD (EMCCD) technology's single-photon sensitivity. As such, CCD220-based cameras are already in use in several modern AO systems [2].

Nüvü Caméras has developed expertise supporting several CCD & EMCCD sensors, including the multi-output configurations with Teledyne-e2v's CCD282, which shares the same split-frame transfer architecture as the CCD220 [3]. This was done at higher readout speeds and with improved noise performances using the patented CCD Controller for Counting Photons (CCCP). At the request of the Gemini Planet Imager team at the Gemini North Observatory, Nüvü Caméras developed the HNü240 camera supporting the CCD220 at previously unattained 30 MHz horizontal readout frequency, enabling faster frame rates and thus better AO performances. The subsequent sections present a comprehensive review of the HNü240's performances and mechanical design, as well as a short preview of applications of interest for the camera.

2. CAMERA PERFORMANCES

2.1 ELECTRONICS

2.1.1 Sensor & Controller Electronics

Teledyne-e2v's CCD220 is an EMCCD sensor designed for high frame rates. This is achieved with the use of a split-frame transfer architecture and multiple outputs. Using 8 outputs at 60 $\times$ 120 pixels/output the CCD220 produces a 240 $\times$ 240 image. The chip architecture is illustrated in figure 1.

Nüvü's CCCP already supports the most common single output Teledyne-e2v EMCCD sensors (*e.g.* CCD97, CCD201-20) and provides several performance advantages compared to other readout electronics. Notably, the CCCP physically

Further author information: E-mail: ebeaulieu@nuvucameras.com, Telephone: +1 514 733 8666

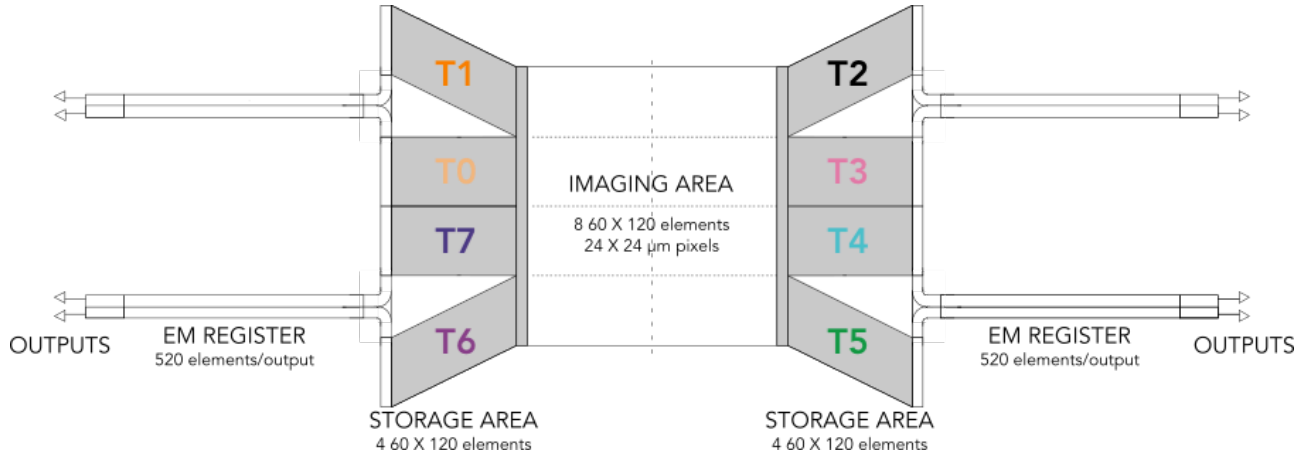

Figure 1. CCD220 chip schematic, as provided by manufacturer Teledyne-e2v, showing the position of the taps as seen by the HNü240. The image is rotated 90° with respect to the horizontal/vertical convention of the CCDs.

generates less noise, specifically Clock Induced Charges (CIC), on the sensors by optimizing the clocks used for charge transfer [4]. This is possible due to the generation of arbitrary waveforms for the control clocks, allowing the selection of the most appropriate clock signal for a specific sensor unit. Moreover, increased control over the clocks allows limiting the CIC increase associated with the use of a higher 30 MHz readout rate; enabling acquisitions at higher frame rates without important degradation of the sensor's typical performances [5].

Supporting the CCD220 with the CCCP electronics was done for the HNü240 camera and was non-trivial due to the significant differences in readout structures to standard sensors. The integration required the use of 2 standard CCCP controllers in a configuration similar to Nüvü Camēras' previous work supporting Teledyne-e2v's CCD282 4k $\times$ 4k EMCCD sensor [3]. The performances achieved with the HNü240 are listed in the following sub-sections.

2.1.2 Frame Rate & Latency

Sensor readout is conducted using a 10 MHz parallel shifting frequency and a 30 MHz pixel readout frequency (14 bits per pixel). This results in a maximum acquisition speed of 3015 frames per second (fps) for a full-frame readout and one overscan line per output to allow for a stable reference for every image. This is the first time this readout speed is achieved on the CCD220 and, at the moment, it is the fastest EMCCD camera available.

Another key metric regarding acquisition speed is latency. Several definitions of latency exist, but one can break it down into several components such as the camera latency, the data transmission latency, and the processing latency. When used with an external trigger in a continuous exposing state between the end of the read-out and the next trigger event, at the very low level the camera latency can be expressed by means of Figure 2. In that figure, the timing to the arrival of the several portions of the image at the camera digital output interface are referred to the external trigger event. On the HNü240, the latency between the trigger event and the first pixel of interest (first pixel of the active image area) is 35.5μs, which includes the time for the initial frame transfer (12.3 μs, moving the image from the imaging area to the storage on the EMCCD), the internal EMCCD pipelining (19.45 μs, for the 8 lines of pipeline represented by 528 horizontal elements and the vertical line transfers), the latency of the Analog-to-digital converter (ADC) and of the data pipelining of the camera's FPGA (3.75 μs). Following that initial latency, the lines of data will come out at a rate of 2.43 μs per line. All in all, 130 lines have to be shifted out of of the horizontal register to fully read the array, and an additional overscan line is added to the read-out. From those numbers, the several latencies can be inferred, as depicted in Table 1.

2.1.3 Noise Performances

The measurements for all noise specifications are taken individually for each output tap as they all have different responses. The Read-out Noise (RON) is measured using the Photon Transfer Curve (PTC) method, which involves shining a stabilized light source on the sensor and progressively increasing exposure time to increase the number of photons received by the sensor. An example of the PTC is shown in figure 3.

Table 1. Acquisition latencies

Start event	End event	Latency (μs)
Trigger	First pixel valid	35.5
Trigger	First line completed	37.9
Trigger	Last line completed	332.3
Beginning of exposure	Last line completed	652.3
Middle of exposure	Last line completed	492.3

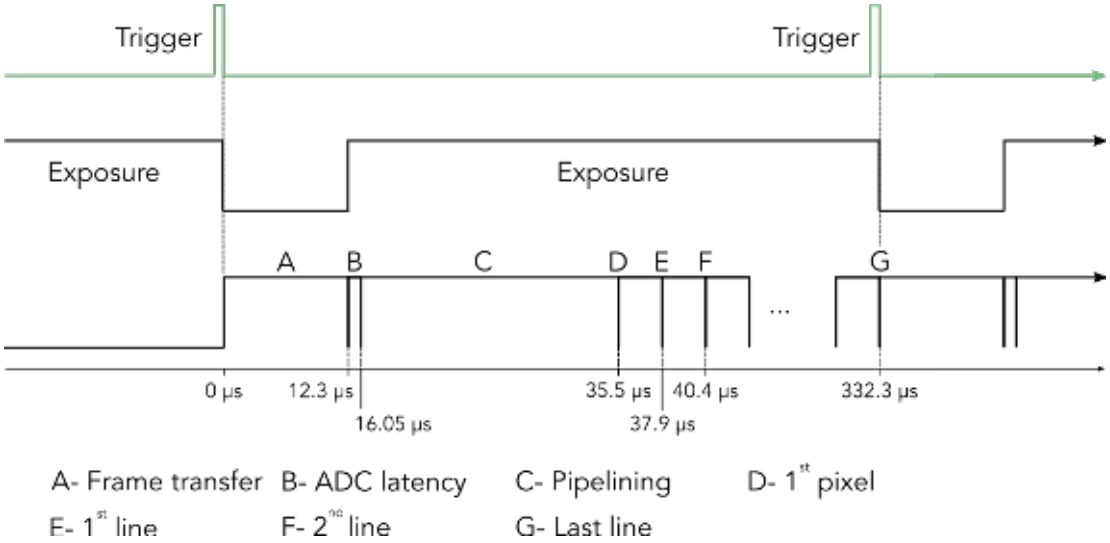

Figure 2. Illustration of the frame transfer timeline (events not spaced to scale).

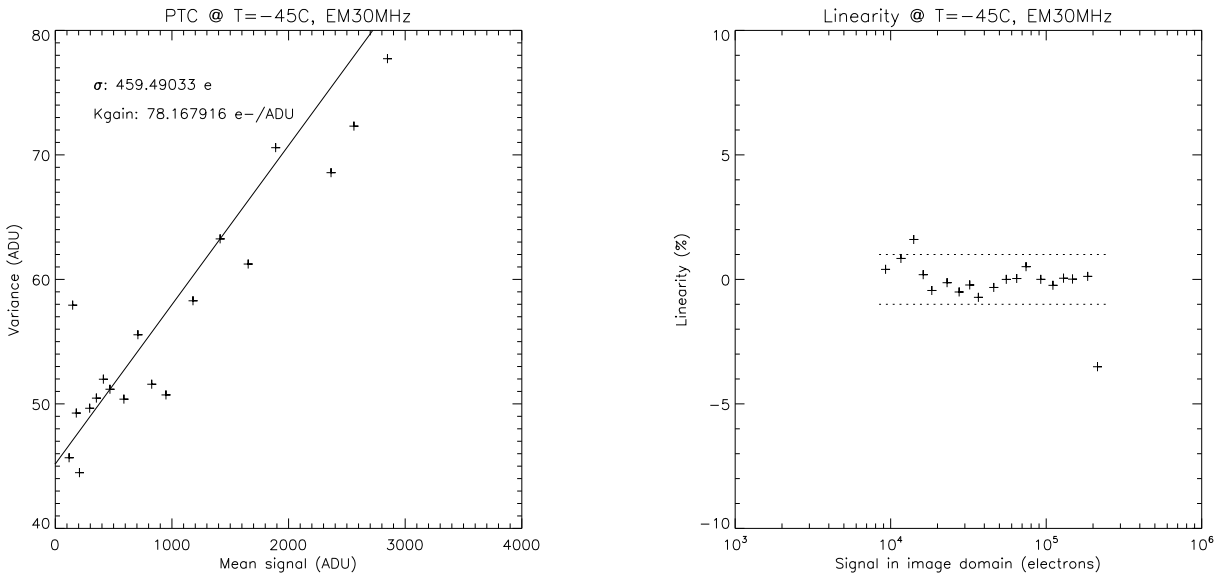

Figure 3. **Left**: Photon transfer curve for one output. **Right**: Linearity for one output.

The CIC is measured by taking dark images at zero exposure time with both horizontal and vertical overscan. The dark current is measured by taking dark frames with increasing exposure time. Considering data from both these measurements, dark current and CIC are disentangled as described in more detail in other papers [3, 6].

The Charge Transfer Efficiency (CTE) is measured with dark frames at high Electron Multiplying (EM) Gain. This is done by identifying bright pixels, which originated from an electron of either dark current or CIC, and comparing their brightness to that of their immediate neighbour. The relative difference in brightness allows to determine the proportion of deferred charges. With this information and the number of elements across which the pixel is transferred to the output register (564 on average), the CTE can be computed. Again here, more details are available in previous papers [3, 5].

Table 2 details noise performances obtained with the HNü240.

Table 2. Detailed HNü240 noise performances, at -45°C, 3015 fps

Output tap	RON (G=1, e^-)	RON (G=5000, e^-)	Background signal (G=1000, e^-/pixel/frame)	Background signal (G=5000, e^-/pixel/frame)	Horiz CTE (G=5000)
T0	340	0.14	0.0011	0.0094	0.99999562
T1	458	0.18	0.0021	0.0074	0.99999188
T2	443	0.17	0.0007	0.0156	0.99999499
T3	457	0.11	0.0009	0.0138	0.99999737
T4	345	0.10	0.0005	0.0085	0.99999654
T5	358	0.11	0.0026	0.0081	0.99999570
T6	427	0.16	0.0017	0.0141	0.99999693
T7	453	0.16	0.0006	0.0127	0.99999640

2.2 INTERFACE

2.2.1 Communication

The HNü240 is compatible with either CameraLink (CL) Full or 10 Gigabit Ethernet (GigE) fiber optics communication schemes to accommodate the necessary data transfer speed. The camera is controlled either through a user interface (NüPixel) or with a documented C++ Software Development Kit (SDK). This allows to readily adjust acquisition parameters such as exposure time, EM Gain or triggering mode and to save images. Notably, Regions of Interest (ROIs) can also be used to increase acquisition speeds though there are some restrictions related to the multiple outputs of the CCD220. These software solutions are compatible with Windows or Linux (Ubuntu or CentOS).

2.2.2 Pixel packing scheme

Although the bandwidth of the CL Full interface if sufficient to carry the entirety of the 3k fps the HNü240 can generate, there are some restrictions imposed by the CL standard that requires the data to be formatted in a particular way. For instance, the CL standard does not support 8 taps of 16 bits, which is what the CCD220 requires. The closest data layout is 8 taps of 8 bits, which means 64 bits of data being transmitted at every CL clock cycle.

The CL Full involves sending the 8x8-bits on three different channels, two of 24 bits (called X and Y), and one of 16 bits (called Z)[7]. In order to keep the data flow symmetric, however, only the X and Y channels could be used by the HNü240. That way, the data of four outputs are sent over the X channel, the data of the remaining four outputs are sent over the Y channel, and the Z channel is left unused. With four 16-bits outputs running at 30 MHz representing 1920 Gbps, and since the maximum frequency of CL is 85 MHz, which provides 2040 Gbps for each of the X and Y channel, it follows that the 16-bits pixels have to be packed over the 24-bits bus width to avoid overloading the CL.

In order to pack the 16-bits pixels of four outputs over a 24-bits wide data link one have to create a pattern that will repeat every time an output has been read three times, and the sending of that data will require 8 CL clock cycles. That way 12 pixels will be packed on a single CL channel over 8 CL clock cycles, since one would be sending 1.5 pixel every clock cycle. Hence, when taking into account both the X and Y channels, 24 16-bits pixels will be transferred every 8 CL clock cycles (Table 3).

Table 3. HNü240 pixel packing of 3 pixels for each tap on the CameraLink bus. `TApB` denotes pixel `B` of tap `A`.

Channel/Clock	Bits [0..7]	Bits [8..15]	Bits [16..23]
X0	T0p0 LSB	T0p0 MSB	T1p0 LSB
Y0	T4p0 LSB	T4p0 MSB	T5p0 LSB
Z0	unused	unused	N/A
X1	T1p0 MSB	T2p0 LSB	T2p0 MSB
Y1	T5p0 MSB	T6p0 LSB	T6p0 MSB
Z1	unused	unused	N/A
X2	T3p0 LSB	T3p0 MSB	T0p1 LSB
Y2	T7p0 LSB	T7p0 MSB	T4p1 LSB
Z2	unused	unused	N/A
X3	T0p1 MSB	T1p1 LSB	T1p1 MSB
Y3	T4p1 MSB	T5p1 LSB	T5p1 LSB
Z3	unused	unused	N/A
X4	T2p1 LSB	T2p1 MSB	T3p1 LSB
Y4	T6p1 LSB	T6p1 MSB	T7p1 LSB
Z4	unused	unused	N/A
X5	T3p1 MSB	T0p2 LSB	T0p2 MSB
Y5	T7p1 MSB	T4p2 LSB	T4p2 MSB
Z5	unused	unused	N/A
X6	T1p2 LSB	T1p2 MSB	T2p2 LSB
Y6	T5p2 LSB	T5p2 MSB	T2p2 LSB
Z6	unused	unused	N/A
X7	T2p2 MSB	T3p2 LSB	T3p2 MSB
Y7	T6p2 MSB	T7p2 LSB	T7p2 MSB
Z7	unused	unused	N/A

Table 4. HNü240 pixel packing of 3 pixels for each tap in the memory when grabbing in CL full, 8x8-bits taps. `TApB` denotes pixel `B` of tap `A`.

16-bits word #	Bits [0..7]	Bits [8..15]
0	T0p0 LSB	T0p0 MSB
1	T1p0 LSB	T4p0 LSB
2	T4p0 MSB	T5p0 LSB
3	unused	unused
4	T1p0 MSB	T2p0 LSB
5	T2p0 MSB	T5p0 MSB
6	T6p0 LSB	T6p0 MSB
7	unused	unused
8	T3p0 LSB	T3p0 MSB
9	T0p1 LSB	T7p0 LSB
10	T7p0 MSB	T4p1 LSB
11	unused	unused
12	T0p1 MSB	T1p1 LSB
13	T1p1 MSB	T4p1 MSB
14	T5p1 LSB	T5p1 MSB
15	unused	unused
16	T2p1 LSB	T2p1 MSB
17	T3p1 LSB	T6p1 LSB
18	T6p1 MSB	T7p1 LSB
19	unused	unused
20	T3p1 MSB	T0p2 LSB
21	T0p2 MSB	T7p1 MSB
22	T4p2 LSB	T4p2 MSB
23	unused	unused
24	T1p2 LSB	T1p2 MSB
25	T2p2 LSB	T5p2 LSB
26	T5p2 MSB	T6p2 LSB
27	unused	unused
28	T2p2 MSB	T3p2 LSB
29	T3p2 MSB	T6p2 MSB
30	T7p2 LSB	T7p2 MSB
31	unused	unused

When grabbing that data over the CL Full interface organized as 8x8-bits taps, and processing it as 16-bits integers, one will get the data organized in the memory as shown in Table 4 in a pattern that repeats every 512 bits. The HNü240 makes sure that the state machine responsible of the pixel packing is reset at the beginning of every line, which allows the data to be processed on a line per line basis independently, without having to take into account the state of the previous line ending.

When one tries to generate a coherent image from the eight taps of the HNü240, the read-out direction of the taps also has to be taken into account. As seen on Figure 1, taps T1 and T7 are horizontally mirrored with respect to taps T0 and T6 , taps T2 and T4 are horizontally mirrored with respect to taps T3 and T5 , and taps T2 , T3 , T4 , and T5 are vertically mirrored with respect to taps T0 , T1 , T6 , and T7 .

2.2.3 Advanced Acquisition Modes

Alternatively, users can control the camera through serial commands to bypass Nüvü's SDK. Though it involves additional work, this allows direct access to pixel-by-pixel information rather than having to wait for the full image information, which is highly relevant in applications where latency needs to be minimized, such as AO.

2.3 PERFORMANCES SUMMARY

Table 5 presents a summary of the general performances of the HNü240.

Table 5. HNü240 performances

Measurement	Specification
Readout Rate	30 MHz
Maximum full Frame Rate	3015 fps
First Pixel Latency	35.5 μs
Peak Quantum Efficiency	94%
Operating Temperature	-45°C
Maximum EM Gain	5000
Effective RON at EM Gain 5000	$\leq$0.2 e
Background signal at 3015 fps, EM Gain 1000	$\leq$0.0015 e/pixel/frame
Horizontal CTE at EM Gain 5000	$\geq$0.99999
Linearity	$\leq$1%

Compared to other EMCCD cameras available on the market, the HNü240 presents the highest frame rate with a 30 MHz readout of the 8 outputs and its latency is lower than other CCD220-based cameras [8]. This makes the HNü240 ideal for high-speed applications. Despite higher readout speeds, the HNü240 also presents an extremely low noise profile. Effective RON is minimal thanks to the maximum EM gain of 5000 and CIC is on par with even the most sensitive EMCCDs which use significantly slower readout rates. These performances allow usage of the camera in light-starved contexts, notably with high-efficiency photon counting acquisitions with signals $\leq$1 photon/pixel/frame. While dark current isn't as significant a factor to the noise profile in high-speed acquisitions, cooling down to -45°C allows to keep dark current low.

3. MECHANICAL SPECIFICATIONS

3.1 PHYSICAL DIMENSIONS

The physical dimensions & layout of the HNü240 are detailed in figure 4. With minimal loss of space inside the unit, the camera dimensions are 232.4 mm (L), 76 mm (W), 175 mm (H).

3.2 COOLING SOLUTION & THERMAL CHARACTERISTICS

The sensor and readout electronics of the camera are cooled using a fully liquid heat dissipation design. This entirely prevents unwanted airflow from fans, which would be incompatible with AO applications. The cooling solution maintains the sensor at -45 °C. The camera was also designed with a sealed body to further prevent thermal exchanges, which could create airflow or upset the sensitive optical bench conditions. The body is filled with argon and is purgeable/refillable.

Despite these design considerations, there is the possibility that sections of the camera casing could heat up preferentially during use. These hot spots can generate a small convective air movement around the EMCCD and so they must not be

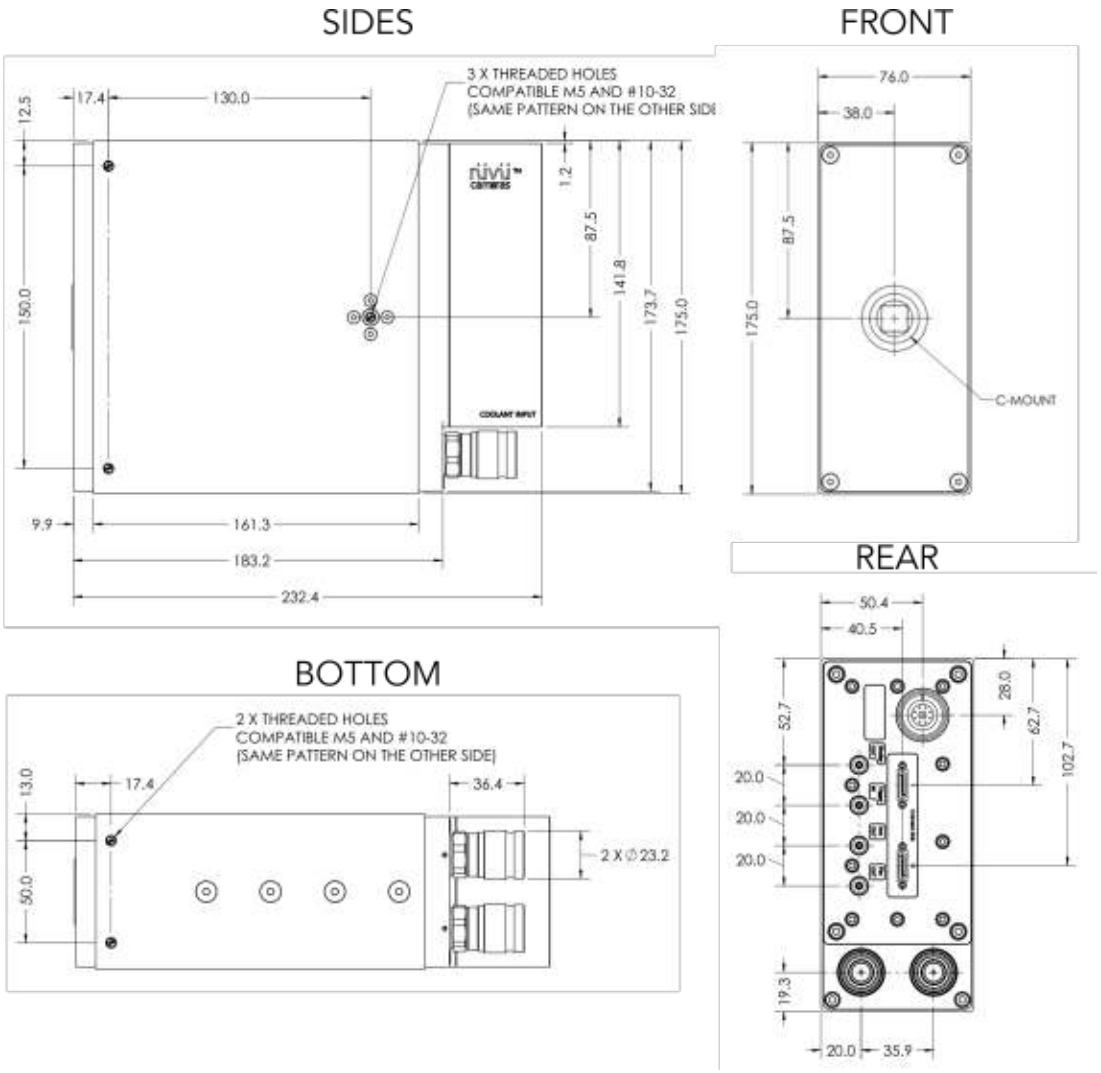

Figure 4. Technical drawings of the HNü240 camera (CL communication model). Dimensions are shown in millimeters.

neglected during system design. Figure 5 shows the HNü240 captured using an infrared camera after running at maximum frame rate for 4 hours, representing an intensive use case. It can be noted that no thermal gradient is observed on the unit, which conforms to the intended design of the camera.

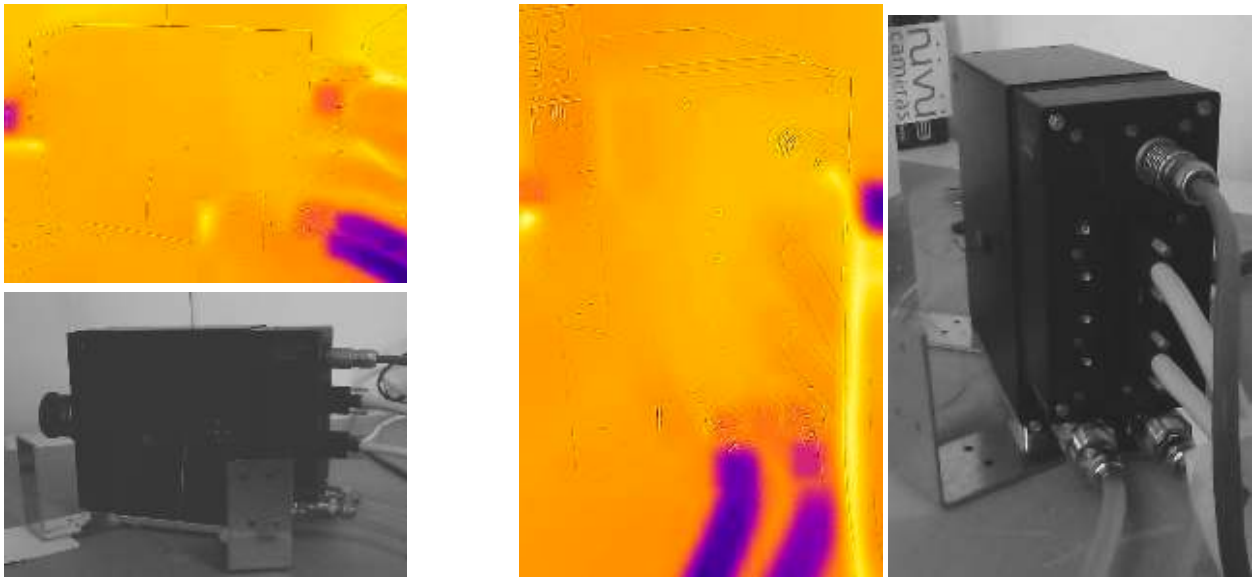

Figure 5. Thermal imaging showing the camera and the water circuits that are 3°C below ambiant. Corresponding visible light images are shown as a reference. **Left**: Side of the camera, showing a very uniform temperature on the camera body and no difference with respect to the ambiant furniture. **Right**: Back of the camera, emphasizing the water circuit and the power cord (warmer than the body).

3.3 OPTICAL CONFIGURATION

The CCD220 sensor integrated into the HNü240 is delivered encased in a sealed integral Peltier package to allow easy cooling. The manufacturer, Teledyne-e2v, specifies a distance of 4mm between the sensor plane and the sapphire window. To minimize reflective losses, Nüvü's design ensured there is no additional window in the optical path.

This design also allows the user to place optics as close as possible to the sensor, which makes the camera compatible with a wide variety of components and affords more flexibility in an instrument's optical design. For more general usage, the camera is outfitted with standard C-mount threading. Thanks to this design, there is no need to use custom or specialized optical components.

4. APPLICATIONS

4.1 CORONAGRAPH FOR EXOPLANET DETECTION

One major challenge associated with the observation of extra-solar planets is the light emitted by their neighbour star. Not only is the brightness of the stellar host $\sim$ 5 to 10 orders of magnitudes higher than that of the planet, but the angular separation between both objects is also very small [9].

To overcome these limitations, one technique makes use of a coronagraph which's purpose is to block the light of the star to allow the observation of fainter objects. While there are many coronagraph types in use at the moment, to achieve high contrast imaging the light feeding the coronagraph must crucially have a highly stable wavefront [10, 11].

As such, AO must be used to correct the wavefront of the incident light. With high-performance AO, it is possible to image planet/star pairs with higher contrast; opening the door to imaging a wider variety of Earth-like planets.

4.2 QUANTUM KEY DISTRIBUTION

With the ever-closer advent of quantum computers, the need to establish secure & high throughput communication links is increasingly pressing. To get ahead of this problem, institutions are focusing on quantum-secure communication which is established through rigorous Quantum Key Distribution (QKD) protocols.

Much research has been done on QKD and we are seeing working systems and proof-of-concept communication over several kilometers of optical fiber around the world [12]. However, modern communication networks do not rely entirely on ground-based connections; a large factor is also space-based communication with satellites.

Any optical communication with a satellite is affected by atmospheric turbulence. For high-sensitivity applications, such as QKD, it is particularly important to minimize the error associated with these perturbations [13]. Using AO to correct for these effects not only makes a strong case for the feasibility of large-scale implementation of these systems but also increases their possible individual data throughput.

4.3 SPACE SITUATIONAL AWARENESS

Space Situational Awareness (SSA) is an increasingly relevant field, as the reliance on satellites and the number of space debris orbiting the planet increase concurrently. Deeper knowledge of the orbital environment is crucial to protect space devices.

Identifying & accurately tracking objects is subject to several hurdles. Notably smaller & faster objects are faint and have very low pixel dwell time, which makes them particularly difficult to detect; especially when their location is unknown.

Using AO to improve image quality will help characterize known objects, allowing for more precise orbit determination, and also increase the resolution of the system to distinguish objects in close proximity [14].

Additionally, the sensitivity of the camera is a significant factor in the detection of new debris, as EMCCDs can not only be used for wavefront sensing for science imaging. Since the pixel dwell time is very short, when not operating in tracking mode, as is often the case for uncharacterized objects, the EMCCD's speed and sensitivity can be leveraged to acquire bursts of images. Combined with post-processing movement compensation, this enables to increase Signal-to-Noise Ratio (SNR) the effective exposure time without increasing the background signal, which is not the case with more standard streak imaging [15]. Nüvü's redesigned electronics also offer a distinct advantage in this performance aspect.

4.4 ADVANTAGES FOR ADAPTIVE OPTICS

AO is often at the core of all these applications, as it is key to achieving the required imaging performances for these science goals. WFS is a crucial part of all AO projects and is where the camera's performances come into play. The HNü240 can help push this technology further thanks to several key performance metrics.

Firstly, the readout of the CCD220 at a 30 MHz readout rate allows frame rates up to 3000 fps. This higher imaging speed allows a faster AO loop which translates to more accurate real-time corrections of the science images. Nüvü's controller technology also ensures sufficient sensitivity to detect faint signals with high SNR even at very low exposure times.

Secondly, a larger sensor allows for more flexibility and higher performance for the AO system. For a Shack-Hartmann WFS, a larger number of lenses can be used on the array which in turn collects correction data in more locations of the image; enabling the use of more precise deformable mirrors with a larger number of actuators and improving correction quality.

This is also illustrated with pyramidal WFS, which is seeing rising interest as the need for better correction in AO increases. While Shack-Hartmann WFS can use a smaller number of pixels, pyramidal WFS is more restrictive. The prism splits the signal into 4 pupil images which should all contain more pixels than the number of actuators on the deformable mirror of the system. Teledyne-e2v's previous high-speed EMCCD detector was comprised of 128 $\times$ 128 pixels which were insufficient for efficient use of pyramidal WFS. However, the CCD220 is all indicated for this application, with a 240 $\times$ 240 sensor that allows a number of pixels that better corresponds to the capabilities of modern deformable mirrors.

While the HNü240 is just finishing up development, Nüvü's HNü128 (128 $\times$ 128 sensor) models are still widely used in Shack-Hartmann WFS systems. Even with fewer pixels, frame rates up to 1.5k fps are adapted to many projects [15–19].

5. CONCLUSION

Nüvü Cameras successfully integrated Teledyne-e2v's CCD220 to the CCCP 30 MHz readout electronics to create the HNü240 EMCCD camera, specifically designed with AO performances in mind. The HNü240 achieves what is currently the highest EMCCD frame rate available at 3015 fps in a full 240 $\times$ 240 pixel frame with a first-pixel latency of 35.5 μs. It also performs at sub-electron RON with an EM Gain up to 5000 (effective RON of $\leq$0.2 e), along with a very low background signal of $\leq$0.0015 e/pixel/frame at maximum frame rate & operating temperature of -45°C. The HNü240's body is sealed, fully liquid-cooled and avoids any significant thermal gradients with ambient air, a key feature for AO systems.

These performance specifications place the HNü240 at the cutting edge of WFS and make it all indicated for the next generation of AO systems which continuously require higher correction quality. Its standard optical path and compact form factor also make for straightforward integration into existing systems requiring lower noise or higher frame rates, enabling upgraded capabilities.

ACKNOWLEDGMENTS

Nüvü Caméras would like to thank the Canadian Space Agency for their contribution to this project under the STDP – AO 6.

REFERENCES

[1] Shi, F., Cady, E., Seo, B.-J., An, X., Balasubramanian, K., Kern, B., Lam, R., Marx, D., Moody, D., et al., "Dynamic testbed demonstration of wfirst coronagraph low order wavefront sensing and control (lowfs/c)," in [*Techniques and Instrumentation for Detection of Exoplanets VIII*], **10400**, 74–90, SPIE (2017).

[2] Hippler, S., "Adaptive optics for extremely large telescopes," *Journal of Astronomical Instrumentation* **8**(02), 1950001 (2019).

[3] Daigle, O., Turcotte, J., Artigau, É., and Doyon, R., "Preliminary characterization results of a large format 4k x 4k emccd," in [*High Energy, Optical, and Infrared Detectors for Astronomy VIII*], **10709**, 68–84, SPIE (2018).

[4] Daigle, O., Gach, J.-L., Guillaume, C., Lessard, S., Carignan, C., and Blais-Ouellette, S., "Cccp: a ccd controller for counting photons," in [*Ground-based and Airborne Instrumentation for Astronomy II*], **7014**, 2288–2297, SPIE (2008).

[5] Daigle, O., Djazovski, O., Francoeur, M., Laurin, D. G., and Doyon, R., "Emccds: 10 mhz and beyond," in [*High Energy, Optical, and Infrared Detectors for Astronomy VI*], **9154**, 104–115, SPIE (2014).

[6] Daigle, O., Djazovski, O., Laurin, D., Doyon, R., and Artigau, É., "Characterization results of emccds for extreme low-light imaging," in [*High Energy, Optical, and Infrared Detectors for Astronomy V*], **8453**, 10–18, SPIE (2012).

[7] "Specifications of the camera link interface standard for digital cameras and frame grabbers," Tech. Rep. 1, http://www.imagelabs.com/wp-content/uploads/2010/10/CameraLink5.pdf (October 2000).

[8] Meeker, S. R., Truong, T. N., Roberts, J. E., Shelton, J. C., Fregoso, S. F., Burruss, R. S., Dekany, R. G., Wallace, J. K., Baker, J. W., et al., "Design and performance of the palm-3000 3.5 khz upgrade," in [*Adaptive Optics Systems VII*], **11448**, 192–204, SPIE (2020).

[9] Marois, C., Gerard, B., Thompson, W., Dong, R., Metchev, S., van der Marel, N., Sivanandam, S., Baron, F., Rowe, J., et al., "Exoplanet imaging: a technological and scientific road-map for finding life signatures on other worlds.," *Canadian Long Range Plan for Astronomy and Astrophysics White Papers* **2020**, 58 (2019).

[10] Mawet, D., Pueyo, L., Lawson, P., Mugnier, L., Traub, W., Boccaletti, A., Trauger, J. T., Gladysz, S., Serabyn, E., et al., "Review of small-angle coronagraphic techniques in the wake of ground-based second-generation adaptive optics systems," in [*Space Telescopes and Instrumentation 2012: Optical, Infrared, and Millimeter Wave*], **8442**, 62–82, SPIE (2012).

[11] Guyon, O., "Imaging earth-like planets around late-type stars with low-inner working angle piaa coronagraphy," in [*Techniques and Instrumentation for Detection of Exoplanets VI*], **8864**, 406–413, SPIE (2013).

[12] Zhang, Q., Xu, F., Chen, Y.-A., Peng, C.-Z., and Pan, J.-W., "Large scale quantum key distribution: challenges and solutions," *Optics express* **26**(18), 24260–24273 (2018).

[13] Oliker, M. D. and Gruneisen, M. T., "How much value does adaptive optics add to a satellite qkd uplink?," in [*Quantum Technologies and Quantum Information Science V*], **11167**, 10–19, SPIE (2019).

[14] Bennet, F., Rigaut, F., Price, I., Herrald, N., Ritchie, I., and Smith, C., "Ao corrected satellite imaging from mount stromlo," in [*Adaptive Optics Systems V*], **9909**, 348–353, SPIE (2016).

[15] Watanabe-Brouillette, K., Daigle, O., Gosselin, Y., Beaulieu, E., and Thibault, S., "Emccd for future sda applications," in [*Sensors and Systems for Space Applications XV*], **12121**, 141–152, SPIE (2022).

[16] Salama, M., Ziegler, C., Baranec, C., Liu, M. C., Law, N. M., Riddle, R., Henry, T. J., Winters, J. G., Jao, W.-C., et al., "An adaptive optics census of companions to northern stars within 25 pc with robo-ao," *The Astronomical Journal* **163**(5), 200 (2022).

[17] Hagelberg, J., Restori, N., Wildi, F., Chazelas, B., Baranec, C., Guyon, O., Genolet, L., Sordet, M., and Riddle, R., "Kalao the swift adaptive optics imager on the 1.2 m euler swiss telescope in la silla, chile," in [*Adaptive Optics Systems VII*], **11448**, 1460–1467, SPIE (2020).

[18] Ogane, H., Akiyama, M., Oya, S., and Ono, Y., "Atmospheric turbulence profiling with a shack-hartmann wavefront sensor," in [*Adaptive Optics Systems VII*], **11448**, 1514–1523, SPIE (2020).

[19] Keskin, O., Jolissaint, L., Bouxin, A., and Yesilyaprak, C., "Troia adaptive optics system for dag telescope," in [*Adaptive Optics Systems VII*], **11448**, 403–417, SPIE (2020).